

Molecular Dynamics of Polymyrcene: Rheology and Broadband Dielectric Spectroscopy on a Stockmayer Type A Polymer

Ciprian Iacob,* Matthias Heck,* and Manfred Wilhelm*



Cite This: *Macromolecules* 2023, 56, 188–197



Read Online

ACCESS |



Metrics & More

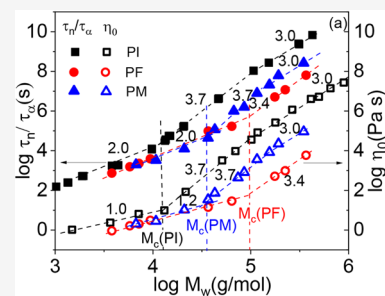


Article Recommendations



Supporting Information

ABSTRACT: Molecular dynamics of polymyrcene (PM) covering a wide range of molecular weights from $6.7 \times 10^3 \leq M_w \leq 3.47 \times 10^5$ g/mol (weight-average molecular weight M_w) with a molar mass dispersity $\mathcal{D} \leq 1.16$ were investigated by oscillatory shear rheology and broadband dielectric spectroscopy. The analysis of the zero-shear viscosity (η_0) versus molecular weight in a double-logarithmic plot reveals a scaling exponent of ~ 1.2 below the critical molecular weight and ~ 3.7 above a critical molecular weight of $M_c \cong 4.4 \times 10^4$ g/mol. However, at molecular weights greater than the reptation molecular weight M_r , a molecular weight substantially larger than the entanglement molecular weight M_e , the zero shear viscosity scaling decreases. A scaling of $\eta_0 \propto M^{3.0}$, which might be attributed to a pure tube-reptation behavior, was found. The exponent of 1.2 is attributed to a Rouse-like dynamic and is interpreted in terms of PM's bottlebrush-like nature arising from tightly packed C6/C8 pendant groups. Dielectric spectroscopy measurements revealed two relaxation processes typical for fully amorphous glassy polymers: The first is a segmental mode process, with a dynamic glass transition process (α), due to the segmental motions and the second one is a local relaxation process in the glassy state (β). Additionally, above the glass transition temperature at low frequency, another relaxation process was observed, which appears to be the normal mode process (n) due to the fluctuation of the end-to-end vector. This polymer is assigned to be a new Stockmayer type A polymer, whose normal mode relaxation is strongly dependent on its molecular weight. These findings allow for the rare possibility to explore the global dynamics of PM by using both oscillatory shear rheology and broadband dielectric spectroscopy methods over a wide range of temperatures to investigate molecular dynamics using the time–temperature superposition principle.



typical for fully amorphous glassy polymers: The first is a segmental mode process, with a dynamic glass transition process (α), due to the segmental motions and the second one is a local relaxation process in the glassy state (β). Additionally, above the glass transition temperature at low frequency, another relaxation process was observed, which appears to be the normal mode process (n) due to the fluctuation of the end-to-end vector. This polymer is assigned to be a new Stockmayer type A polymer, whose normal mode relaxation is strongly dependent on its molecular weight. These findings allow for the rare possibility to explore the global dynamics of PM by using both oscillatory shear rheology and broadband dielectric spectroscopy methods over a wide range of temperatures to investigate molecular dynamics using the time–temperature superposition principle.

INTRODUCTION

Today there is a growing interest in modern polymer chemistry toward the development of bio-based and biocompatible polymers as well as renewable alternatives to petrochemical-based materials.^{1–5} One of the most used bio-based polymers is polyisoprene, frequently applied in the rubber industry as natural rubber. In addition to *cis*-1,4-polyisoprene, natural rubber, attractive renewable feedstocks include the family of acyclic terpenes as monomers (especially monoterpenes (C10) and sesquiterpenes (C15)), which offer an extensive variety of chemical structures.^{6–8} Among these, 7-methyl-3-methylene-octa-1,6-diene, C₁₀H₁₆, or β -myrcene can be a further promising bio-based alternative as monomers for specific applications, e.g., in rubber science due to its low glass transition temperature T_g (see Table 1) and thus deserves further investigation. To our knowledge, the polymerization of myrcene was first described as early as 1913, but the polymer itself was not investigated in terms of polymer physics.⁹ Polymyrcene (PM; see Figure 1) or its derivatives may replace petrochemically sourced polymers or shares of such polymers, for example, the soft block of thermoplastic elastomers.^{10–12} As one example, β -myrcene can be naturally found in bay leaves, hop, wild thyme, and ylang ylang fruits and is produced on a large scale as one of the products of the pyrolysis of turpentine oil at 450–600 °C (≈ 37000 t/year).^{13,14} Because β -myrcene possesses an anioni-

Table 1. Weight-Average Molecular Weights M_w , Dispersity \mathcal{D} as Determined by SEC, and Glass Transition Temperatures from DSC, Rheological Measurements (LVE), and Broadband Dielectric Spectroscopy (BDS)^a

| sample ID | M_w (g/mol) | \mathcal{D} | $T_{g,DSC}$ (K) | $T_{g,LVE}$ (K) | $T_{g,BDS}$ (K) |
|-----------|---------------|---------------|-----------------|-----------------|-----------------|
| PM6.7 | 6700 | 1.14 | 205 | 206 | 205 |
| PM10.7 | 10700 | 1.11 | 205 | 205 | 206 |
| PM11.6 | 11600 | 1.11 | 207 | 208 | 209 |
| PM36.6 | 36600 | 1.11 | 208 | 208 | 209 |
| PM42.9 | 42900 | 1.13 | 208 | 208 | 208 |
| PM74.1 | 74100 | 1.12 | 207 | 208 | 208 |
| PM85.6 | 85600 | 1.12 | 208 | 208 | 208 |
| PM115.9 | 115900 | 1.13 | 208 | 209 | 209 |
| PM155.1 | 155100 | 1.13 | 208 | 208 | 208 |
| PM192 | 192000 | 1.12 | 208 | 209 | 209 |
| PM347.7 | 347700 | 1.16 | 208 | 208 | 209 |

^aSee the text below for details about the T_g determination.

Received: September 10, 2022

Revised: December 15, 2022

Published: December 28, 2022



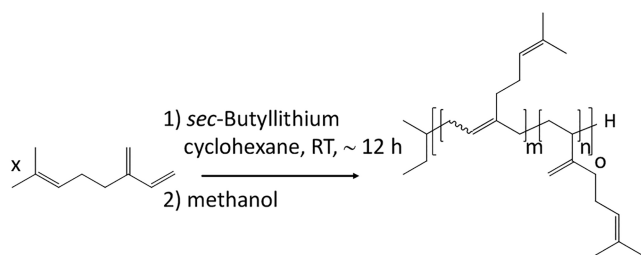


Figure 1. Anionic polymerization of myrcene in cyclohexane using *sec*-BuLi as an initiator. Under these experimental conditions more than 90 mol % of the 1,4-isomer was obtained (determined by ^1H NMR).

cally polymerizable conjugated diene structure, linear backbone polymyrcene with a high content of *cis*-1,4 units and a narrow molecular weight distribution can be obtained by anionic polymerization if nonpolar solvents are used (see Figure 1).^{5,15–17} Additionally, the C–C double bonds of the side groups make this polymer interesting for further functionalization.¹⁰ Similar to polyfarnesene (PF; see Figure S1 in the Supporting Information),⁸ PM adopts a bottlebrush-like structure with two or four carbon atoms in the backbone but with shorter C6 and C8 tightly spaced side chains (see the scheme in Figure 1 or Figure S1), where the side arms are not entangled due to their small size.¹⁸ Additionally, similar to the structure of *cis*-1,4-polyisoprene or *cis*-1,4-polyfarnesene, PM possesses components of the repeating unit electrical dipole moment parallel along and perpendicular to the main chain, which can be classified as Stockmayer type A and Stockmayer type B dipoles, respectively.¹⁹ The polarization in an electrical field, which is the sum of the dipole moments of individual monomer units, gives information about the end-to-end vector of the whole polymer chain.²⁰ The fluctuations of the end-to-end vector allow to investigate the global chain dynamics, which are also reflected in the terminal regime of temperature-dependent master curves determined in oscillatory shear rheological measurements.^{21–23}

This article represents a detailed study of the molecular dynamics of polymyrcene with different, defined molecular weights, which is crucial for a correlation of molecular weight and material properties, analyzed by a combination of rheological and dielectrical measurements.⁹

EXPERIMENTAL SECTION

Materials and Methods. Secondary butyllithium (*sec*-BuLi, 1.4 mol/L in hexane, Sigma-Aldrich), butyllithium (*n*-BuLi), calcium hydride, and 1,1-diphenylethylene (DPE, 98%, Alfa Aesar) were used as received without any purification. Cyclohexane (99%, Fisher) was stirred over calcium hydride for several days. To remove traces of water, *sec*-BuLi and DPE were added. The red color of the solution displays the absence of water. Methanol (>98.5%, VWR Chemicals), which was used for the termination of the polymerization reactions, was frozen with liquid nitrogen and subsequently thawed to remove oxygen. This was necessary to prevent radical formation and a coupling of two growing polymer chains leading to a doubling of the molecular weight during the termination reaction. This procedure was repeated until no more gas bubbles were observed. Myrcene (90%, tech., Acros Organics) was dried by the addition of *n*-BuLi to the monomer until a slight yellow color appeared, indicating the absence of water and the beginning of the polymerization process. Then the monomer was carefully distilled under reduced pressure at approximately 130 °C.

Synthesis of Polymyrcene (PM). Prior to the synthesis of PM, dry cyclohexane (e.g., 100 mL of cyclohexane for 5 g of myrcene) was distilled into the reaction flask. The monomer was then added through a syringe under a counter flow of argon. The polymerization was initiated

by the addition of *sec*-BuLi. A slight yellowish color was observed for high sample concentrations and low molecular weight samples, which means there was a high concentration of macroanions in the reaction flask. The mixture was stirred for 12 h and finally quenched with degassed methanol. The cyclohexane was removed by freeze-drying of the polymer solution.

This procedure leads to a chain microstructure composed of primarily 1,4-*cis* and *trans*-addition products (i.e., C6 pendant groups) and <10 mol % of the 3,4-addition products (C8 pendant units), as determined from 400 MHz ^1H NMR. Samples with molecular weight dispersities \mathcal{D} of 1.11 to 1.16 were obtained. Low dispersities are needed for a correlation of material properties, such as relaxation times, to a respective molecular weight. All polymer samples used in this study are labeled using the abbreviation of the polymer and the weight-average of the molecular weight in kg/mol. For example, a polymyrcene sample with a molecular weight of 6700 g/mol is labeled PM6.7.

Molecular Weight Determination. The PMs were characterized by size exclusion chromatography (SEC) and ^1H NMR to determine the molecular weight of the PM samples and their dispersity \mathcal{D} (see Table 1).

The weight-average molecular weight M_w of the polymer samples was determined via size exclusion chromatography coupled with multiangle laser light scattering (MALLS). The SEC equipment is an Agilent 1200 (Polymer Standard Service, Mainz, Germany). The MALLS unit is a PSS SLD7000/BI-MwA (Brookhaven Instruments). Two PSS SDV Lux 300 \times 8 mm i.d. columns with pore sizes of 10^3 and 10^5 Å were used. The mobile phase was THF stabilized with 250 ppm BHT at 30 °C with a flow rate of 1 mL min^{-1} .

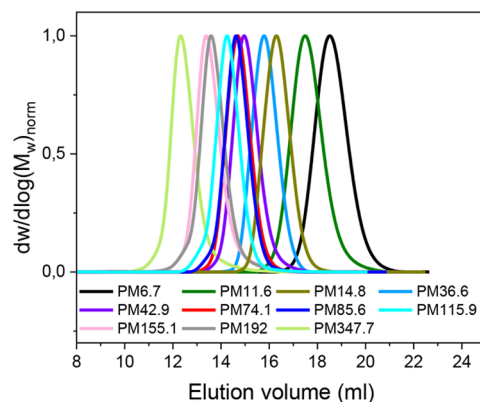


Figure 2. Normalized SEC traces for the PM samples versus the elution volume. The SEC traces determined by the DRI detector are displayed.

The refractive index increment (dn/dc), which was used to calculate M_w , was determined by the measurement of a concentration series with a DnDc-2010 differential refractometer from Brookhaven Instruments Corp. (Holtville, NY). The concentration series consisted of 10 solutions of PM in THF with concentrations ranging from 1.4 to 14.3 g/L. A THF density of $\rho = 0.877$ g/ cm^3 was used, and a dn/dc value of 0.1685 ± 0.0071 mL/g for PM in THF at $T = 30$ °C was determined.²⁴

The total number-average molecular weight M_n was determined by an end-group analysis using ^1H NMR whenever the signal of the end group was sufficient for analysis. For the NMR experiments the samples were dissolved in deuterated chloroform (CDCl_3 , 99.8%, Sigma-Aldrich), and signals were referenced to the solvent peak at δ 7.26 ppm. A Bruker Avance III Microbay 400 MHz spectrometer was used, and 512 scans were performed. Characteristic peaks at 1.59 and 1.67 ppm (methyl groups at C8, 6H; see Figure 3) in relation to peaks at 0.86 ppm (methyl protons of *sec*-BuLi, 6H) were used to calculate M_n of the PM samples (see Figure 3).^{25,26}

Differential Scanning Calorimetry (DSC). Glass transition temperatures (T_g) were determined by differential scanning calorimetry (DSC) using a TA Instruments Q200 differential scanning calorimeter. The experiments were conducted using cooling and

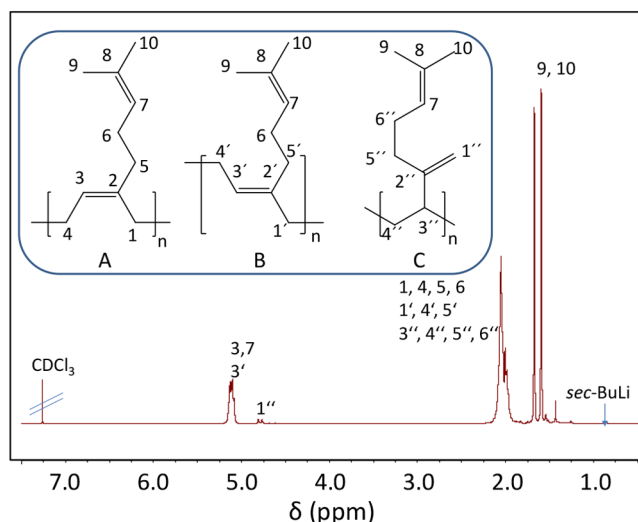


Figure 3. The 400 MHz ^1H NMR spectrum of PM in CDCl_3 (512 scans). Inset: structure of *cis*-1,4-PM (A), *trans*-1,4-PM (B), and 3,4-PM (C).²⁶

heating rates of 10 K/min on samples with a mass $m \sim 10$ mg. The PM samples were dried in a vacuum oven at 343 K prior to the DSC measurements in order to avoid the influence of moisture, residual solvent, and adsorbed impurities. The T_g was determined to be the inflection point of the heat capacity change in the second heating run. Glass transition temperatures for the PMs under study are presented in Table 1.

Density Measurements. The density of the PM samples was measured in order to calculate the entanglement molecular weight M_e by using the Doi and Edwards relation (see eq 2).²⁷ The density was determined at room temperature using a high-precision helium pycnometer AccuPyc II 1340 from Micrometrics Instrument Corporation. The sample chamber was calibrated with different density standards before running each measurement. Prior to the measurements all PM samples were extensively dried and purged in order to avoid the influence of moisture and adsorbed impurities. The reported values of the density represents an average of ten consecutive measurements with a determined standard deviation of 0.002 g/cm³. The obtained densities (ρ) of the PM samples were between 0.89- and 0.91 g/cm³ (see Table S3 in the Supporting Information).

Rheological Measurements. Oscillatory shear measurements were performed on a strain-controlled ARES G2 rheometer (TA Instruments) equipped with a force rebalance transducer capable of measuring a torque of 50 nN·m–200 mN·m. All PM samples were dried under vacuum at a temperature $T = 373$ K for 12 h to remove water and then were loaded onto parallel plates with diameters of 13 and 8 mm for the acquisition of the storage and loss moduli (G' and G''), measured over an angular frequency range of $\omega_1 = 0.1$ –100 rad/s under a nitrogen atmosphere. The strain amplitude γ_0 was selected to be within the linear viscoelastic range, $\gamma_0 < 5\%$. The master curves for the shear moduli G' and G'' were constructed by assuming time–temperature superposition (TTS) at the indicated reference temperature ($T_{\text{ref}} = 293$ K, see Figure 4).

The reference temperature of 293 K was chosen so that a comparison of the zero shear viscosities of the PM samples as a function of molecular weight to the literature data of the dielectric normal mode relaxation times at an isofrictional state²⁸ for polyisoprene (PI) and polyfarnesene (PF) is possible (see also final results in Figure 11). The mechanical segmental relaxation time ($\tau_0 = 1/\omega_1$) at T_{ref} is obtained at the frequency ω_1 , at which the storage G' and the loss G'' moduli cross each other in the glassy state region (see Figure S2). Glass transition temperatures from linear viscoelastic experiments (LVE, $T_{g,\text{LVE}}$; see Table 1) were obtained by the local maximum in G'' , which corresponds to the transition in the shift factors from WLF (Williams–Landel–Ferry) to Arrhenius behavior. The transition from WLF to Arrhenius

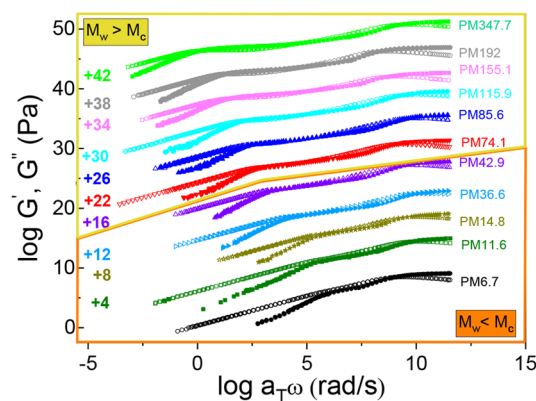


Figure 4. Dynamic rheological master curves of the storage and loss moduli for all PM samples from the terminal region to the glassy state at a reference temperature of $T_{\text{ref}} = 293$ K. The curves were shifted vertically. The scale factors are listed at the left side of the y-axis. The molecular weights of the PM polymers below and above critical molecular weight M_c are also indicated by the line between PM42.9 and PM74.1. The crossing of the storage G' and the loss moduli G'' , from the terminal region to the rubber plateau, in the sample's master curves was used as criteria to distinguish between entangled and unentangled PM samples. In order to make the separation of the samples more clear, the master curves of the two samples (PM42.9 and PM74.1) at the border of critical molecular weight of M_c are compared in Figure S3.

behavior indicates the breakdown of the time–temperature superposition below T_g . The master curve of Figure 5, in which the

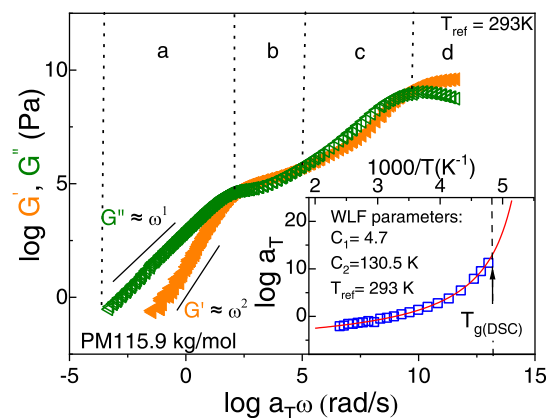


Figure 5. Storage and loss modulus of PM115.9 at $T_{\text{ref}} = 293$ K from the terminal regime (a) via the rubber plateau (b) and the transition zone (c) to the glassy state (d). Inset: horizontal shift factor a_T used to generate the master curve. The solid red line represents fits using the WLF equation. The dashed vertical line represents the glass transition temperature from DSC measurements. In rheological experiments T_g was obtained by the local maximum of G'' at a frequency of 0.01 rad/s.

rheological data are shifted beyond T_g and the Arrhenius behavior of a_T becomes clearly visible, is only shown in the Supporting Information. The $T_{g,\text{LVE}}$ and $T_{g,\text{BDS}}$ are identical with those determined from DSC within experimental uncertainty. For the transition between the Newtonian flow range at low frequencies and the rubbery range at higher frequencies the same procedure can be applied (see Figure S2).²⁹ Relaxation times at another reference temperature can be obtained by $\tau(T_{\text{ref}}) = \tau(T) \log a_T$.

Broadband Dielectric Spectroscopy Measurements. Broadband dielectric spectroscopy (BDS) measurements were performed using a Novocontrol high-resolution Alpha dielectric analyzer Concept 40 over the frequency range of 10^{-1} to 10^7 Hz, aided by a Quattro Cryosystem temperature controller with a temperature stability of $\Delta T <$

0.1 K, under a dry nitrogen atmosphere. Polished gold electrodes with diameters of 15 and 10 mm were placed on the bottom and top of the samples, respectively, to create a parallel plate capacitor cell. Three fused SiO₂ fibers with diameters of 50 μm were used as spacers. The sandwiched polymer films were positioned in the Novocontrol spectrometer. The dielectric permittivity and conductivity were measured isothermally in steps of 10 K using an AC voltage amplitude of 1.5 V over a broad temperature range ranging from 123 to 393 K. This was done in both cooling and heating in order to verify reproducibility. Prior to measurements, each sample was annealed in the Novocontrol sample cell at 393 K in a heated stream of nitrogen for 2 h to remove moisture acquired during sample loading and air bubbles.

RESULTS AND DISCUSSION

The mechanical shear response of polymer melts in the linear regime can provide a clear signature of various processes, such as the melt flow, rubbery plateau, glassy dynamics, and subglass transition relaxations.^{30,31} A crucial component is the combination of measurements at various frequencies and temperatures. To do so, master curves for $T_{\text{ref}} = 293$ K ($T_g + 87$ K) were generated by frequency-scale shifting the isothermal frequency sweep data, within the linear regime, from 393 to 213 K (with increments of 10 K) for all PM samples, as shown in Figure 4. Analyzing Figure 5, which displays the master curve of PM115.9, two relaxation processes can be clearly determined in the rheological data: the lower frequency process (around $\omega_1 = 1$ rad/s) is attributed to the chain relaxation, while the higher frequency relaxation (around $\omega_1 = 10^9$ rad/s) is associated with the segmental relaxation (α -process). Time–temperature superposition (TTS) works well (for the temperatures above T_g) for the LVE spectra, and the segmental relaxation is confirmed to be associated with the observed α -process by fitting the temperature dependence of the frequency-scale horizontal shift factors (a_T) with the WLF equation. The frequency shift factors between 393 and 213 K are well fitted by the WLF equation. The glass transition temperature can be quantified from rheometry data by the local maximum in G'' (around $\omega_1 = 10^{10}$ rad/s at $T_{\text{ref}} = 293$ K) because the loss modulus defines the relaxation process. To approximate a frequency-independent T_g , the data were shifted to a low angular frequency such as 0.01 rad/s. Alternatively, the peak in $\tan \delta (= G''/G')$ can be used to determine T_g , or the Vogel–Fulcher temperature from the WLF fit ($T_g = 50$ K + T_0). The Vogel–Fulcher temperature T_0 is the temperature, at which the system deviates from the equilibrium, where the domain of cooperativity grows toward the infinite size at the Kauzmann zero entropy temperature.^{32–35} A tabulated summary of the quantitative agreement of the glass transition temperatures ($T_{g,\text{DSC}}$, $T_{g,\text{LVE}}$, and $T_{g,\text{BDS}}$) for all samples in this work is shown in Table 1.

The insets in Figures 5 and 6 show the correlation between the horizontal shift factors a_T and the inverse temperature for the PM samples.

The temperature dependence of the experimental multiplicative horizontal shift factors, a_T , used to construct the master curves in Figures 4 and 5 obeyed the WLF equation given by

$$\log a_T = -\frac{C_1(T - T_{\text{ref}})}{C_2 + T - T_{\text{ref}}} \quad (1)$$

where C_1 and C_2 are nearly universal constants that depend mainly on the relative difference to T_g , respective the chosen reference temperature T_{ref} which is 293 K in the specific case. The a_T shift factors for all PM samples collapse onto a single

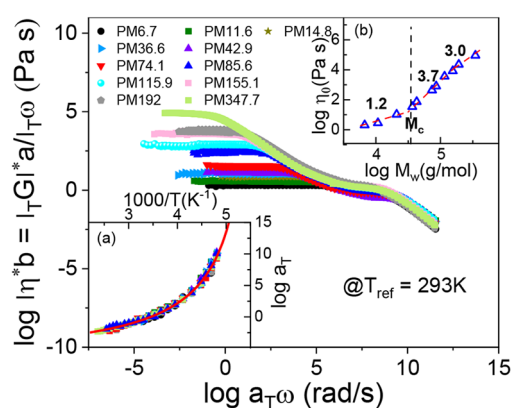


Figure 6. Complex viscosity versus reduced frequency for the PM samples at $T_{\text{ref}} = 293$ K. Insets: (a) Frequency shift factors (a_T) used to generate the master curves. The solid red line represents fits using the WLF equation. (b) Zero shear viscosities at $T_{\text{ref}} = 293$ K as a function of M_w for the PM materials. The dotted vertical line represents the approximate critical molecular weight $M_c \cong 4.4 \times 10^4$ g/mol for PM. Slope values are also indicated.

curve, which can be described by a single WLF curve (solid red line in the insets of Figures 5 and 6). The fact that TTS is obeyed implies that the segmental dynamics of the polymer chains show a strong dependence on T . The best fit curve to the data using the WLF equation gives $C_1 = 4.7$ and $C_2 = 130.5$ K (at $T_g + 87$ K). The fit parameter C_1 correlates the mobility of the polymer chains at T_{ref} to their maximal mobility. The parameter C_2 reflects the non-Arrhenius character of the polymer and represents a measure of the fragility that classifies the polymers in “strong” and “fragile” according to the Angell plot.^{36,37} Normally, the values of the horizontal shift factors, a_T , at T_g should be zero if $T_{\text{ref}} = T_g$; in our case, a_T is greater than 12 because our T_{ref} was chosen to be 293 K intentionally in order to compare the zero shear viscosities (η_0 , measured via oscillatory shear and applying the Cox–Merz rule) of PMs at 293 K with dielectric normal mode relaxation times at an isofrictional state for polyisoprene (PI) and polyfarnesene (PF) (see their comparison in Figure 11). At isofrictional conditions, the normal mode relaxation is normalized to the segmental relaxation in order to eliminate a large influence on η_0 caused by only small differences in T_g .

In order to quantify the relaxation times determined from BDS and LVE in Figure S2, we analyzed the molecular dynamics of PM samples where we demonstrated that there is a good coincidence of the terminal relaxation times obtained from LVE measurements and normal-mode relaxation times obtained from dielectric spectroscopy.

Figure 6 shows the absolute value of the complex viscosities ($|\eta^*|$) versus the reduced frequency ($a_T \omega$) constructed at $T_{\text{ref}} = 293$ K for all PM samples under investigation. The zero shear viscosities, measured at low shear rates, are obtained from the plateau of the reduced complex viscosity plotted against reduced frequency ($a_T \omega$). These values are displayed as a function of M_w at $T_{\text{ref}} = 293$ K in the inset (b) of Figure 6. The zero shear rate viscosity (zero shear viscosities, η_0) is widely used as a fundamental descriptor of the flow resistance of polymer melts characterizing both the rheological response at a low stress as well as low shear rates and the influence of the molecular architecture on the resistance to flow. For the case of amorphous flexible linear polymer melts it is well-known that the dynamics of short polymer chains are governed solely by the Rouse

behavior, while that of long chains follows a reptation behavior due to the presence of physical entanglements.^{38–40} Consequently, according to the tube model by de Gennes⁴¹ and Doi and Edwards,⁴² the prediction for the scaling of the zero-shear viscosity η_0 is expected to depend approximately linear on the molecular weight for low molecular weights. The viscosity depends directly on the molecular weight of the chain M_w if $M_w < M_c$ (specific critical molecular weight). For $M_w > M_c$ the molecular weight dependence of the zero-shear viscosity increases $\eta_0 \propto M_w^{3.4}$. For a molecular weight $M_w > M_r$ the zero-shear viscosity shows the following dependence $\eta_0 \propto M_w^{3.36,37}$. M_r is the reptation molecular weight, which is defined within this article as the molecular weight at which the experimental viscosity reverts to the expected M_w^3 dependence and is based on a combination of reptation and constraint release. As seen in the inset (b) of Figure 6, the dynamics of entangled polymyrcene chains display a transition in the slope of $\log \eta_0$ versus $\log M_w$ to $\alpha = 3.7 \pm 0.3$ at higher molecular weights, indicative of the transition to entangled chain dynamics. The dynamics of entangled chains are understood in terms of reptation and the characteristic limiting processes, including the contour length fluctuations, originally proposed by Doi,⁴² and the constraint release.⁴³ The effect of these competing processes in the transition regime between Rouse and pure reptation dynamics may reflect the different values of the power law from the prediction for the scaling of η_0 with molecular weight. This can be seen in experimental data at $T_{ref} = 293$ K of the zero-shear viscosity as a function of molecular weight of polyisoprene and polybutadiene polymer melts, which shows for the entangled region $\eta_0 \propto M_w^{3.7}$ and $\eta_0 \propto M_w^{3.29}$, respectively.⁴⁰ While the dynamics of entanglements at higher M_w are observed by the rubbery plateau and the presence of the crossover of G' and G'' as observed in Figure 5 for PM115.9 and Figure 4 from PM74.1 to PM347.7. A further, second transition, denoted by M_r ($M_r = 190550$ g/mol, with the number of entanglements $Z = 10$), is observed from entangled behavior due to pure reptation (Figure 6). Nevertheless, considering the relatively modest number of PM samples explored in this molecular weight range, the pure reptation molecular weight should be used with caution. The tube model by Doi and Edwards predicts that the large-scale dynamics of chains in an amorphous linear polymer melt emerge simply from a fundamental length scale called the tube diameter interpreted as the end-to-end distance of entanglements.³⁹ Experimentally, M_c is determined from the plateau modulus G_n^0 , known as the signature of entanglements during stress–relaxation, that can be obtained from the elastic G' modulus from the master curve in the rubbery region. In case G' did not exhibit a clear plateau, G_n^0 was determined from the value of G' around the middle of the elastic plateau between the two intersections of G' and G'' below and above the rubber plateau at the minimum of $\tan \delta$:^{39,40}

$$M_e = \rho RT / G_n^0 \quad (2)$$

where ρ (≈ 0.91 g/cm³) is the polymer density, R is the ideal gas constant, and T is the reference temperature, at which G_n^0 was determined. The measured values for the density of all PM samples can be found in Table S3. The preceding equation establishes a clear relationship between microscopic, chemistry-dependent details and the global chain dynamics of polymer melts. The value of the plateau of the elastic G' modulus in Figure 5 is $G_n^0 = 124.4$ kPa, and consequently we obtain a value of $M_e = 17800$ g/mol. The obtained value for PM's M_e is between those of PI ($M_e = 5 \times 10^3$ g/mol) and PF ($M_e = 5 \times 10^4$ g/mol)

and is similar to the polymyrcene entanglement molecular weight reported by Fetters et al.⁴⁴ The molecular weight M of the related monomers is $M = 68.12$ g/mol for isoprene, $M = 136.23$ g/mol for myrcene, and $M = 204.36$ g/mol for farnesene.

Typical dielectric spectra for the dielectric loss at selected temperatures and as a function of frequency are presented in Figure 7. Clearly, three relaxation processes are observed for

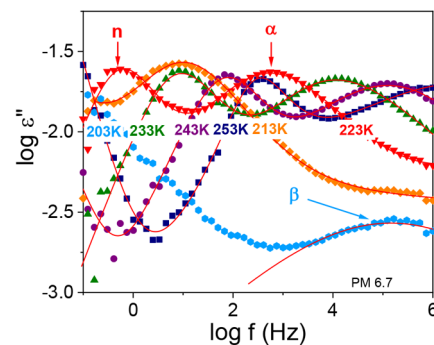


Figure 7. PM 6.7 dielectric loss spectra at selected temperatures as indicated versus frequency. Three relaxation processes are observed: the normal mode (n), the α -relaxation, and the β -relaxation. The solid lines represent the HN fits.

PM: the frequency corresponding to the peak in the imaginary part of the loss spectra ϵ'' at high temperature and rather low frequency is related to the chain, which can relax by what is known as the dielectric normal mode (n), reflecting the fluctuation of the end-to-end vector characterizing the global chain dynamics. The n relaxation follows a non-Arrhenius behavior and is mainly influenced by M_w (see Figure 10). At lower temperatures the second dipolar-like relaxation is observed, which is related to the segmental dynamics or dynamic glass transition process (α) of the polymer and is often well described by the empirical Havriliak–Negami (HN) function in the frequency domain.²⁹ The α -process and the dielectric normal mode process are resolved by fitting two HN functions to the two relaxation processes (see Figure 7). The empirical HN function with additional conductivity contribution is^{29,45,46}

$$\epsilon^*(\omega) = \epsilon_\infty + \sum_{j=2} \frac{\Delta\epsilon}{[1 + (i\omega\tau_{HNj})^m]^n} - i \left(\frac{\sigma_0}{\epsilon_0\omega} \right)^s \quad (3)$$

where σ_0 is the dc conductivity, ω is the angular frequency of the external applied electric field, s is the exponent describing conductivity slope and should ideally be 1, ϵ_0 is the permittivity in free space, $\Delta\epsilon$ is the dielectric relaxation strength of the j process, τ_{HNj} is the HN characteristic relaxation time related to τ_{max} , m (that is inversely related to the width of the relaxation) and n (that is the high-frequency asymmetry parameter) are the shape parameters, and j is the index over which the relaxation processes are summed. The secondary relaxation spectra (β -relaxation processes) were analyzed using a symmetric Cole–Cole function (corresponding to a shape parameter $\beta = 1$ in the HN equation). The characteristic relaxation times for each process were estimated as the reciprocal of the peak frequency $\tau = 1/2\pi f_{max}$. The α -relaxation time (obtained by fitting the peak in the imaginary part of the loss spectra at different temperatures by using the HN function) follows a non-Arrhenius behavior and is mainly influenced by the temperature. Although T_g s of the

PM samples are not very different, the T_g increases slightly as the degree of polymerization increases followed by a saturation at high molecular weights. This small molecular weight dependence of T_g is well-known for polymers and can be described by the so-called Flory–Fox equation.^{8,47–49} The third relaxation process, on the high-frequency side and below T_g , is attributed to a local relaxation in the glassy state (β), and its temperature evolution follows an Arrhenius behavior.

The use of the horizontal (frequency) axis shift principle to describe the polymer behavior over an extended frequency range, as applied to rheological data, can also be applied to dielectric spectroscopy data. However, this principle is often not used because of the already extremely broad frequency range accessible to dielectric spectroscopy techniques at a single measured temperature, at which 8–9 decades in frequency can be measured, compared to rheology where usually around 3–4 decades are measured. Nevertheless, this principle in dielectric spectroscopy should be used with caution; this method works reasonably in a limited frequency range, but some parts of the shifted data corresponding to different relaxation processes does not overlap (e.g., the peaks of the secondary β -relaxation process); this behavior is related to different temperature dependencies of the relaxation times of the respective processes. The dielectric modulus has mainly been used for the construction of the dielectric master curves when compared to the results of mechanical spectroscopy. This was demonstrated by Kremer et al. for the case of PI, where the comparison of temperature dependencies of the relaxation times obtained from the two methods indicates a very good coincidence of the terminal relaxation times determined by rheology and the normal mode relaxation times determined from dielectric measurements.²⁹ Similar agreement between the relaxation times in the master curves constructed from rheological and dielectric measurements are also observed for PM115.9 (see Figure S2).

In order to show the dielectric spectral shape of the α -peak and the normal mode with temperature, we plot in Figure 8 the

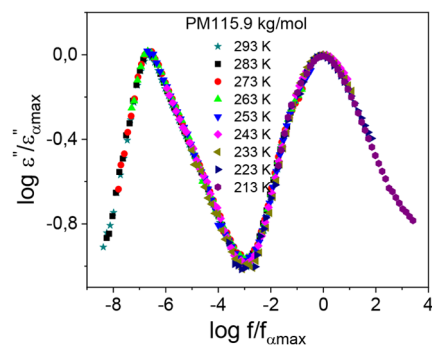


Figure 8. Rescaled dielectric spectra for PM115.9 for indicated temperatures, where ϵ'' is rescaled by the maximum height $\epsilon''_{\alpha,\max}$ and f by the frequency $f_{\alpha,\max}$ of the α -peak.

dielectric spectra of PM115.9 and in Figure 9 the dielectric spectra for all PMs in this study, for which $\log \epsilon''/\epsilon''_{\alpha,\max}$ is plotted versus rescaled frequency $\log f/f_{\alpha,\max}$ where $\epsilon''_{\alpha,\max}$ and $f_{\alpha,\max}$ are the height and the frequency, respectively, of the alpha peak. The rescaled dielectric data in Figure 8 show the segmental mode process and the dynamic glass transition process (α) at $\log f/f_{\alpha,\max} = 0$. The peak below this value is related to the normal mode relaxation process where $\log f/f_{\alpha,\max} = -7$. As expected, for

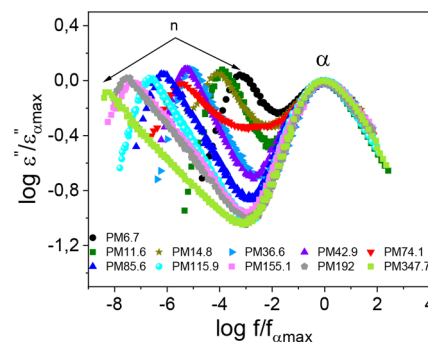


Figure 9. Rescaled dielectric spectra of polymyrce samples investigated: PM6.7 ($T = 213$ – 233 K), PM11.6 ($T = 213$ – 243 K), PM14.8 ($T = 223$ – 233 K), PM36.6 ($T = 223$ – 253 K), PM42.9 ($T = 233$ – 253 K), PM74.1 ($T = 233$ – 263 K), PM85.6 ($T = 243$ – 273 K), PM115.9 ($T = 233$ – 293 K), PM155.1 ($T = 263$ – 283 K), PM347.7 ($T = 273$ – 293 K): dielectric permittivity ϵ'' rescaled by its α -peak height $\epsilon''_{\alpha,\max}$ and f rescaled by the frequency $f_{\alpha,\max}$ of the α -peak.

higher M_w , the normal mode process for all PM samples shifts to lower reduced frequencies. In the frequency range of the α -process the data agree well, and one can observe that the envelope of the α -peak is temperature and molecular weight independent. For one sample, namely PM74.1, a broad α -peak is observed, where the left wing is following a different behavior with respect to the other samples for reasons not known yet. One may suspect the molecular weight dispersity to play a role in the peak broadness; however, according to Table 1, PM74.1 has a \mathcal{D} of 1.12, which is similar to the other polymer samples. The peak position of the normal mode seems to be between PM42.9 and PM85.6, in agreement with measured M_w s.

Figure 10 shows the relaxation rates of the glassy state, segmental relaxations and the normal mode relaxation as a

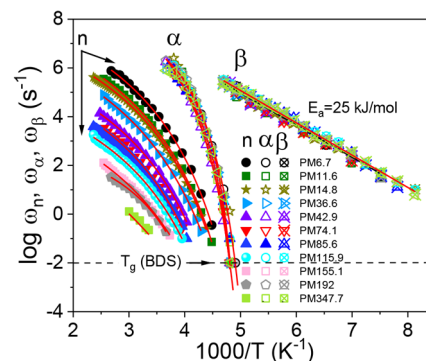


Figure 10. Relaxation rates for the glassy state β -relaxation, ω_β , the segmental relaxation process, ω_α and the normal mode relaxation, ω_n , for PM with different M_w versus $1000/T$. The solid lines are VFT and Arrhenius fits. The dashed line labeled T_g (BDS) indicates the extrapolation of the VFT fits to $1/\omega = 100$ s. The VFT fit parameters are presented in Table S2. The T_g values obtained from BDS measurements are similar to those from LVE and DSC within experimental uncertainty (see Table 1).

function of the inverse temperature. The glassy state β -relaxation (ω_β) processes are observed below T_g and coincide for all PM samples under study, reflecting a similar motion. Analyzing further the activation plot, the temperature evolution of the β -relaxation peak follows an Arrhenius behavior, $\omega_\beta(T) = \omega_0 \exp(-E_a/RT)$, with an activation energy of $E_a = 25$ kJ/mol. We speculate that the origin of the β -relaxation processes is

connected to the polymyrcene side group motions in the glassy state. Because the polymyrcene structure consists of two or four carbon atoms in the backbone repeat unit and C6 or C8 (see Figure 3), as a pendant group, it is expected that at high molecular weights the chains adopt a cylindrical bottlebrush-like structure with tightly spaced side chains similar to a previously studied bottlebrush-like polymer, namely polyfarnesene, PF.⁸ Given that the backbone units of PF are identical with PM and have slightly longer pendant groups consisting of C11 and C13, we may expect PF to display a higher activation energy of its side group motions compared to PM. This is indeed confirmed as the activation energy of PF was found to be $E_a = 28$ kJ/mol, which supports our hypothesis regarding the origin of the β -relaxation processes.⁸ Turning to the activation plot for the different processes, displayed in Figure 10, at higher temperatures, the segmental relaxation seems to follow a Vogel–Fulcher–Tammann (VFT) temperature dependence, typical for the most glassy polymer systems. The empirical Vogel–Fulcher–Tammann equation is given as $\omega_\alpha = \omega_\infty \exp(-BT_0/T - T_0)$ where $\omega_\infty = \tau_\infty^{-1}$, the high-temperature limit of the relaxation rate; B is a constant related to fragility—a measure of the extent of deviation from the Arrhenius dependence and T_0 is the Vogel temperature, which typically lies about 50 °C below the glass transition temperature.⁵⁰

On the basis of B values from Table S2, PM is considered as a fragile glass. The VFT fit parameters are presented in Table S2. The α -process for all materials is very similar and covers relaxation rates over more than 7 decades ($\omega/2\pi = 10^{-1}$ – 10^6 Hz) and 4 decades in the inverse temperature, $1000/T$.

The glass transition temperatures obtained from the dielectric measurements, $T_{g,BDS}$, are determined by VFT fits of the mean structural relaxation rates ω_α vs $1000/T$ extrapolated to the value $1/\omega = 100$ s, which is an empirical relation (the T_g values of the intersection of the extrapolated VFT curve with the horizontal line at 100 s) that is used for obtaining the T_g by broadband dielectric spectroscopy and correlates well with T_g s from DSC measurements. The values of $T_{g,BDS}$ are in agreement with the T_g s obtained from LVE and DSC measurements and are all listed in Table 1.

A slight increase of T_g (from 205 to 209 K) with M_w is observed for low-molecular-weight samples due to the influence of end-group contributions; higher molecular weight samples are less influenced by the end-group contributions. In contrast to the α - and β -relaxation processes, the normal mode relaxation process observed at high temperatures is as expected highly dependent on the molecular weight of PM covering 2 orders of magnitude of molecular weights and 7 decades in relaxation rates. On the basis of the chemical structure of PM and its adopted conformation, where the electrical dipole moment is parallel along the polymer backbone, we attribute this relaxation processes to the normal mode relaxation originating from the collective polymer dynamics.⁴⁷ The normal mode relaxations seems to follow for each molecular weight sample a VFT temperature dependence, typical for the cooperative processes of Stockmayer type A polymers.

The ratio τ_n/τ_α of the normal mode τ_n and the α -relaxation time τ_α as a function of the molecular weight M_w of PM compared to linear polyisoprene (PI)^{51–53} and polyfarnesene (PF)⁸ is included in Figure 11. This approach of the data representation is known as an isofrictional condition, where the molecular weight dependence of the monomeric friction coefficient is given by the temperature dependence of the normal mode relaxation normalized by the segmental relaxation

of each material at a fixed temperature. Further in Figure 11b normalization of M_w to the M_c allows a comparison of the unentangled–entangled transition for each polymer melt (PI, PM, and PF). This can also be seen by the inflection point of the complex viscosity ($\frac{d^2 \log \eta^*}{d(\log a_T \omega)^2}$) in Figure 6 and the normal mode relaxation times at an isofrictional state of the different polymers collapsing onto each other. At the same time, the zero-shear viscosity experimentally demonstrates the universality of the polymer melts' dynamics, which is highlighted by the three regimes of their dynamical behavior as the molecular weight increases: the Rouse regime, the entanglement regime, and an indicated pure reptation regime. Additionally, the comparative representation of M_w normalized to the M_c of the respective polymers can be found in the Supporting Information (Figure S5).

In Figure 11 three power-law regions for two polymers, namely PI and PM, can be observed. PF shows just two regimes:

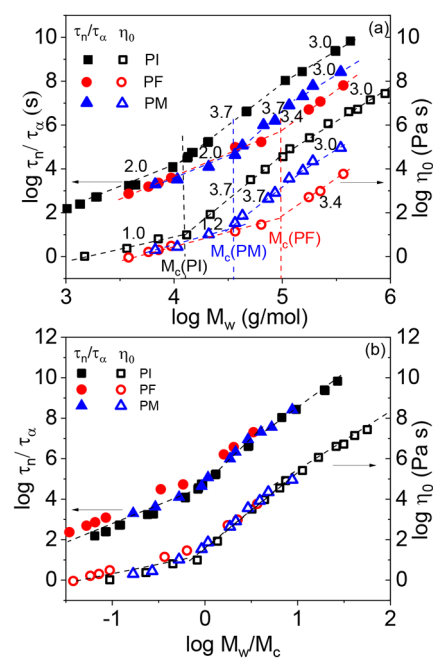


Figure 11. Solid symbols: dielectric normal mode relaxation times for polyisoprene (PI: square symbols, reproduced from refs 28 and 51–53), polyfarnesene (PF: circle symbols, reproduced from ref 8), and polymyrcene (PM: triangle symbol) versus (a) M_w at an isofrictional state and (b) normalized M_w/M_c . Open symbols: zero shear viscosities at $T_{ref} = 293$ K as a function of (a) M_w and (b) normalized M_w/M_c for the PI,⁴⁰ PF,⁸ and PM materials. The dotted vertical lines represent the approximate critical molecular weight M_c for PI, $M_{c(PI)} \cong 10^{4.2}$ g/mol $\cong 1.6 \times 10^4$ g/mol, PF $M_{c(PF)} \cong 10^5$ g/mol, and PM $M_{c(PM)} \cong 10^{4.6}$ g/mol $\cong 4.4 \times 10^4$ g/mol. Slope values are also indicated.

Rouse dynamics and an entanglement region. The pure reptation regime was not reached in the case of PF because of the lack of high- M_w synthesized samples with narrow molecular weight dispersity. The ratio τ_n/τ_α was observed to be $\propto M_c^z$, with $z = 2$ in the Rouse dynamic region, $z = 3.4$ and 3.7 for the entangled region, and the transition from the first region to the second region. This is associated with the entanglement molecular weight with $M_c \cong 10^{4.2}$ g/mol ($\cong 1.6 \times 10^4$ g/mol) for PI,^{29,51,54–56} and $M_c \cong 10^{4.6}$ g/mol ($\cong 4 \times 10^4$ g/mol) and $M_c \cong 10^5$ g/mol for PM and PF, respectively.⁸ Note that $z = 2$ was

also observed by other studies of the dielectric normal mode for linear PI.⁵⁶ The experimental finding of M_c of PM is between M_c of PI and PF (its monomer is an isoprene trimer) is not surprising; the backbone segments of PM are analogous to isoprene and β -myrcene can be considered an isoprene dimer. Above M_c the entanglement dynamics dominate until the second crossover between entanglement and pure reptation is achieved at $M_r \cong 10^5$ g/mol and $M_r \cong 10^{5.3}$ g/mol ($\cong 2 \times 10^5$ g/mol) for PI and PM, respectively. At higher molecular weights of PM ($>M_r$) z decreases to a value of 3, which could be attributed to a pure tube reptation, but has to be considered with caution due to a low number of data points in this molecular weight range.^{27,41} The relation of M_r to M_c with $M_r = 5M_c$ in the case of PM is small compared to other polymers such as polystyrene ($M_r = 15M_c$), polyisobutylene ($M_r = 25M_c$), polybutadiene ($M_r = 100M_c$), and polyethylene ($M_r = 220M_c$).^{57–60} This may be attributed to the chemical structure like the size of groups attached to the polymer backbone as well as the mobility of the backbone itself. The two polymers PI and PM, which were compared in this study, also show this trend of an increasing M_c/M_r with a decrease in size of the groups attached to the polymer backbone. Accordingly, M_r of PI is 6.25 its M_c . The polymer polybutadiene, whose backbone is the same as for PI and PM but does not carry any group, additionally confirms this trend. In order to illustrate the comparison of the normal mode at isofrictional conditions to the chain relaxation, in Figure 11 also $\log \eta_0$ versus M_w is presented. In the low- M_w regime, $M_w < M_c$, the slope of PM samples is $\cong 1.2 \pm 0.03$, indicating a Rouse-like behavior up to $M_c \cong 1.6 \times 10^4$ g/mol; this slope is very similar to that found for bottlebrush polymers with atactic polypropylene (a-PP) side chains synthesized via ring-opening metathesis polymerization using Grubbs third-generation catalyst as well for the case of PF bottlebrush polymers with C11 and C13 pendant groups.^{8,61,62} A simple comparison between these two materials, PF and PM, shows a clear transition from the Rouse to the entangled region, identical with dielectric findings (PM: $M_c \cong 10^{4.6}$ g/mol ($\cong 4.4 \times 10^4$ g/mol) and PF: $M_c \cong 10^5$ g/mol). The M_c of PM and PF is significantly higher than for linear PI where $M_c \cong 10^4$ g/mol; instead, bottlebrush polymers based on atactic polypropylene side chains show no transition to the entanglement region. The bottlebrush polymers based on atactic PP undergo a sphere-to-cylinder conformational transition manifested in the Rouse-like behavior up to $M_w \gg M_c \cong 10^6$ g/mol.⁶¹ The PM pendant groups are much shorter (C6 and C8) than in the case of PF (C11 and C13) and below the entanglement molecular weight of linear PI, making it possible that at high molecular weight ($M_c > 10^{4.6}$ g/mol, $Z \approx 10$) PM behaves like an entangled polymer melt with a large molecular weight between the backbone entanglements. Given the chemical architecture and dynamics of PM over a broad frequency and temperature range, which are similar to those of PF, we conclude that PM behaves like a bottlebrush polymer melt whose normal mode relaxation is strongly dependent on molecular weight as expected for a Stockmayer type A polymer (see Figure 10).

CONCLUSION

In summary, a series of narrowly distributed PM samples in the molecular weight range of $M_w = 6700$ to 347000 g/mol were synthesized, and the molecular chain dynamics of polymyrcene (PM) were investigated by employing oscillatory shear, DSC, and broadband dielectric spectroscopy measurements. The results were compared to structurally similar polymers, but with

shorter and longer side groups such as polyisoprene and polyfarnesene (PF), respectively (see Table 2). Dielectric

Table 2. Comparison of M_c and T_g of the Polyterpenes Polyisoprene, Polymyrcene, and Polyfarnesene^a

| | polyisoprene | polymyrcene | polyfarnesene |
|---------------|--------------|-------------|---------------|
| M_c (g/mol) | 5000 | 17800 | 50000 |
| T_g (K) | 212 | 208 | 198 |

^aThe values are associated with the cis-1,4 isomer of the polymers under comparison. The values for PI and PF are taken from the literature.^{8,54}

measurements establish that PM is a new Stockmayer type A polymer, exhibiting a global end-to-end relaxation process strongly dependent on M_w . Considering the zero shear viscosities as a function of M_w for the polymyrcene series, we found the scaling exponents of ~ 1.2 , corresponding to the Rouse-like dynamics and ~ 3.7 above a critical molecular weight ($M_c \cong 10^{4.6}$ g/mol $\cong 4.4 \times 10^4$ g/mol), corresponding to the entanglement regime ($M_c/M_e \sim 2-4$). This deviation of the scaling exponent in the unentangled regime from the expected value of 1 seems to be related to the bottlebrush-like nature of PM and PF, which both carry densely packed groups. Above M_c , PM behaves as an entangled polymer melt, with a molecular weight between backbone entanglements of $M_e = 1.78 \times 10^4$ g/mol. At molecular weights much larger than the reptation molecular weight ($M_w \gg M_r$, number of entanglements Z ca. 10), similar to the linear homopolymers, a scaling exponent of the zero shear viscosities on M_w of ~ 3 is found, which could be attributed to a pure reptation, but has to be considered with caution due to a large error resulting from only a single data in this molecular weight range.

ASSOCIATED CONTENT

Supporting Information

The Supporting Information is available free of charge at <https://pubs.acs.org/doi/10.1021/acs.macromol.2c01884>.

Figure S1: chemical structure of the monomers and their respective polymers; Table S1: isomer contents determined by 400 MHz ¹H NMR (512 scans); Table S2: VFT fitting parameters of the normal mode and α -segmental relaxations of the PM samples; Table S3: density values determined for each of the PM samples; Figure S2: electrical and mechanical master curves for PM115.9 and temperature dependence of the segmental and chain relaxation times determined from dielectric spectra and chain relaxation from mechanical spectra; Figure S3: dynamic master curves of the storage and loss moduli for the PM samples PM42.9 and PM74.1 and respective van Gurp–Palmen plot of the data; Figure S4: storage and loss modulus of PM115.9 beyond T_g indicating the breakdown of TTS at T_g ; Figure S5: dielectric normal mode relaxation times and zero shear viscosities for polyisoprene, polyfarnesene, and polymyrcene versus Z , the number of entanglements at an isofrictional state; Figure S6: rheodielectrics setup and rheodielectric kit used for measurements (PDF)

Enlarged versions of figures in this article (ZIP)

AUTHOR INFORMATION

Corresponding Authors

Ciprian Iacob – Institute for Chemical Technology and Polymer Chemistry, Karlsruhe Institute of Technology, 76131 Karlsruhe, Germany; National Research and Development Institute for Cryogenic and Isotopic Technologies, 240050 Rm. Valcea, Romania; orcid.org/0000-0001-7982-0586; Email: Ciprian.Iacob@kit.edu

Matthias Heck – Institute for Chemical Technology and Polymer Chemistry, Karlsruhe Institute of Technology, 76131 Karlsruhe, Germany; orcid.org/0000-0002-7752-1838; Email: Matthias.Heck@kit.edu

Manfred Wilhelm – Institute for Chemical Technology and Polymer Chemistry, Karlsruhe Institute of Technology, 76131 Karlsruhe, Germany; orcid.org/0000-0003-2105-6946; Email: Manfred.Wilhelm@kit.edu

Complete contact information is available at:

<https://pubs.acs.org/10.1021/acs.macromol.2c01884>

Notes

The authors declare no competing financial interest.

ACKNOWLEDGMENTS

The authors gratefully acknowledge the financial support of the DFG (Wi 1911/22-1), AiF-IGF 19925N, and AiF (ZF4016102TA8). C.I. acknowledges the Romanian Ministry of Education and Research, CNCS - UEFISCDI, projects: PN 19110204, PN-III-P1-1.1-TE-2019-1734, and PN3-P3-428-23042021 ERANET-M-SMICE-Li, within PNCDI III. M.H. acknowledges Dr. Szimonetta Heck-Matus for inspiring discussions regarding this project. The authors acknowledge Dr. Michael Pollard and Maxi Hoffmann for the proofreading and valuable comments on the manuscript.

DEDICATION

This article is dedicated to Professor Hans-Wolfgang Spiess on the occasion of his 80th birthday.

REFERENCES

- (1) Sarkar, P.; Bhowmick, A. K. Sustainable rubbers and rubber additives. *J. Appl. Polym. Sci.* **2018**, *135*, 45701.
- (2) Corma, A.; Iborra, S.; Velty, A. Chemical Routes for the Transformation of Biomass into Chemicals. *Chem. Rev.* **2007**, *107*, 2411–2502.
- (3) Zhu, Y.; Romain, C.; Williams, C. K. Sustainable polymers from renewable resources. *Nature* **2016**, *540*, 354–362.
- (4) Gandini, A. Polymers from Renewable Resources: A Challenge for the Future of Macromolecular Materials. *Macromolecules* **2008**, *41*, 9491–9504.
- (5) Tzourtouklis, I.; Hahn, C.; Frey, H.; Floudas, G. Molecular Dynamics and Viscoelastic Properties of the Biobased 1,4-Poly-myrcene. *Macromolecules* **2022**, *55*, 8766–8775.
- (6) Wilbon, P. A.; Chu, F.; Tang, C. Progress in Renewable Polymers from Natural Terpenes, Terpenoids, and Rosin. *Macromol. Rapid Commun.* **2013**, *34*, 8–37.
- (7) Yao, K.; Tang, C. Controlled Polymerization of Next-Generation Renewable Monomers and Beyond. *Macromolecules* **2013**, *46*, 1689–1712.
- (8) Iacob, C.; Yoo, T.; Runt, J. Molecular Dynamics of Polyfarnesene. *Macromolecules* **2018**, *51*, 4917–4922.
- (9) Lautenschläger, C. L. Autoxydation und Polymerisation ungesättigter Kohlenwasserstoffe. Ph.D. Thesis, 1913; Karlsruhe, Techn. Hochsch.
- (10) Matic, A.; Hess, A.; Schanzenbach, D.; Schlaad, H. Epoxidized 1,4-polymyrcene. *Polym. Chem.* **2020**, *11*, 1364–1368.
- (11) Zhou, C.; Wei, Z.; Lei, X.; Li, Y. Fully biobased thermoplastic elastomers: synthesis and characterization of poly(L-lactide)-b-polymyrcene-b-poly(L-lactide) triblock copolymers. *RSC Adv.* **2016**, *6*, 63508–63514.
- (12) Wahlen, C.; Blankenburg, J.; von Tiedemann, P.; Ewald, J.; Sajkiewicz, P.; Müller, A. H. E.; Floudas, G.; Frey, H. Tapered Multiblock Copolymers Based on Farnesene and Styrene: Impact of Biobased Polydiene Architectures on Material Properties. *Macromolecules* **2020**, *53*, 10397–10408.
- (13) Setyawan, H. Y.; Sunyoto, N. M. S.; Wijana, S.; Pranowo, D. Progress on Pine Derivative Products as Fuel Source in Indonesia. *IOP Conference Series: Materials Science and Engineering* **2020**, *811*, 012015.
- (14) Breitmaier, E. *Terpenes: flavors, fragrances, pharma, pheromones*, 1st ed.; Wiley-VCH: Weinheim, 2008.
- (15) Matic, A.; Schlaad, H. Thiol-ene photofunctionalization of 1,4-polymyrcene: Thiol-ene photofunctionalization of 1,4-polymyrcene. *Polym. Int.* **2018**, *67*, 500–505.
- (16) Bolton, J. M.; Hillmyer, M. A.; Hoyer, T. R. Sustainable Thermoplastic Elastomers from Terpene-Derived Monomers. *ACS Macro Lett.* **2014**, *3*, 717–720.
- (17) Grune, E.; Bareuther, J.; Blankenburg, J.; Appold, M.; Shaw, L.; Müller, A. H. E.; Floudas, G.; Hutchings, L. R.; Gallei, M.; Frey, H. Towards bio-based tapered block copolymers: the behaviour of myrcene in the statistical anionic copolymerisation. *Polym. Chem.* **2019**, *10*, 1213–1220.
- (18) Yoo, T.; Henning, S. K. Synthesis and Characterization of Farnesene-Based Polymers. *Rubber Chem. Technol.* **2017**, *90*, 308–324.
- (19) Stockmayer, W. H. Dielectric dispersion in solutions of flexible polymers. *Pure and Applied Chemistry* **1967**, *15*, 539–554.
- (20) Watanabe, H. Dielectric Relaxation of Type-A Polymers in Melts and Solutions. *Macromol. Rapid Commun.* **2001**, *22*, 127–175.
- (21) Höfl, S.; Kremer, F.; Spiess, H.; Wilhelm, M.; Kahle, S. Effect of large amplitude oscillatory shear (LAOS) on the dielectric response of 1,4-cis-polyisoprene. *Polymer* **2006**, *47*, 7282–7288.
- (22) Hyun, K.; Höfl, S.; Kahle, S.; Wilhelm, M. Polymer motion as detected via dielectric spectra of 1,4-cis-polyisoprene under large amplitude oscillatory shear (LAOS). *J. Non-Newtonian Fluid Mech.* **2009**, *160*, 93–103.
- (23) Kardasis, P.; Oikonomopoulos, A.; Sakellariou, G.; Steinhart, M.; Floudas, G. Effect of Star Architecture on the Dynamics of 1,4-cis-Polyisoprene under Nanometer Confinement. *Macromolecules* **2021**, *54*, 11392–11403.
- (24) Baird, Z. S.; Uusi-Kyyny, P.; Pokki, J.-P.; Pedegert, E.; Alopaeus, V. Vapor Pressures, Densities, and PC-SAFT Parameters for 11 Bio-compounds. *Int. J. Thermophys.* **2019**, *40*, 102.
- (25) Glatzel, J.; Noack, S.; Schanzenbach, D.; Schlaad, H. Anionic polymerization of dienes in 'green' solvents. *Polym. Int.* **2021**, *70*, 181–184.
- (26) Sarkar, P.; Bhowmick, A. K. Synthesis, characterization and properties of a bio-based elastomer: polymyrcene. *RSC Adv.* **2014**, *4*, 61343–61354.
- (27) Feldman, D. The theory of polymer dynamics, by M. Doi and S. F. Edwards, the Clarendon Press, Oxford University Press, New York, 1986, 391 pp. *Journal of Polymer Science Part C: Polymer Letters* **1989**, *27*, 239–240.
- (28) Abou Elfadl, A.; Kahlau, R.; Herrmann, A.; Novikov, V. N.; Rössler, E. A. From Rouse to Fully Established Entanglement Dynamics: A Study of Polyisoprene by Dielectric Spectroscopy. *Macromolecules* **2010**, *43*, 3340–3351.
- (29) Kremer, F.; Schönhals, A., Eds.; *Broadband Dielectric Spectroscopy*; Springer: Berlin, 2003.
- (30) Meins, T.; Dingenouts, N.; Kübel, J.; Wilhelm, M. In Situ Rheodielectric, *ex Situ* 2D-SAXS, and Fourier Transform Rheology Investigations of the Shear-Induced Alignment of Poly(styrene-*b*-1,4-isoprene) Diblock Copolymer Melts. *Macromolecules* **2012**, *45*, 7206–7219.

- (31) Gainaru, C.; Figuli, R.; Hecksher, T.; Jakobsen, B.; Dyre, J.; Wilhelm, M.; Böhmer, R. Shear-Modulus Investigations of Mono-hydroxy Alcohols: Evidence for a Short-Chain-Polymer Rheological Response. *Phys. Rev. Lett.* **2014**, *112*, 098301.
- (32) Berthier, L.; Charbonneau, P.; Ninarello, A.; Ozawa, M.; Yaida, S. Zero-temperature glass transition in two dimensions. *Nat. Commun.* **2019**, *10*, 1508.
- (33) Berthier, L.; Ozawa, M.; Scalliet, C. Configurational entropy of glass-forming liquids. *J. Chem. Phys.* **2019**, *150*, 160902.
- (34) Debenedetti, P. G.; Stillinger, F. H. Supercooled liquids and the glass transition. *Nature* **2001**, *410*, 259–267.
- (35) Stillinger, F. H.; Debenedetti, P. G.; Truskett, T. M. The Kauzmann Paradox Revisited. *J. Phys. Chem. B* **2001**, *105*, 11809–11816.
- (36) Angell, C. A. Formation of Glasses from Liquids and Biopolymers. *Science* **1995**, *267*, 1924–1935.
- (37) Angell, C. A.; Ngai, K. L.; McKenna, G. B.; McMillan, P. F.; Martin, S. W. Relaxation in glassforming liquids and amorphous solids. *J. Appl. Phys.* **2000**, *88*, 3113–3157.
- (38) Rouse, P. E. A. Theory of the Linear Viscoelastic Properties of Dilute Solutions of Coiling Polymers. *J. Chem. Phys.* **1953**, *21*, 1272–1280.
- (39) Rubinstein, M.; Colby, R. H. *Polymer Physics*; Oxford University Press: New York, 2003.
- (40) Unidad, H. J.; Goad, M. A.; Bras, A. R.; Zamponi, M.; Faust, R.; Allgaier, J.; Pyckhout-Hintzen, W.; Wischniewski, A.; Richter, D.; Fetters, L. J. Consequences of Increasing Packing Length on the Dynamics of Polymer Melts. *Macromolecules* **2015**, *48*, 6638–6645.
- (41) de Gennes, P. G. Reptation of a Polymer Chain in the Presence of Fixed Obstacles. *J. Chem. Phys.* **1971**, *55*, 572–579.
- (42) Doi, M. Explanation for the 3.4-power law for viscosity of polymeric liquids on the basis of the tube model. *J. Polym. Sci., Polym. Phys. Ed.* **1983**, *21*, 667–684.
- (43) Graessley, W. W. *Synthesis and Degradation Rheology and Extrusion*; Springer-Verlag: Berlin, 1982; Vol. 47; pp 67–117.
- (44) Fetters, L. J.; Lohse, D. J.; Richter, D.; Witten, T. A.; Zirkel, A. Connection between Polymer Molecular Weight, Density, Chain Dimensions, and Melt Viscoelastic Properties. *Macromolecules* **1994**, *27*, 4639–4647.
- (45) Havriliak, S.; Negami, S. A complex plane analysis of α -dispersions in some polymer systems. *Journal of Polymer Science Part C: Polymer Symposia* **1966**, *14*, 99–117.
- (46) Havriliak, S.; Negami, S. A complex plane representation of dielectric and mechanical relaxation processes in some polymers. *Polymer* **1967**, *8*, 161–210.
- (47) Abou Elfadl, A.; Kahlau, R.; Herrmann, A.; Novikov, V. N.; Rössler, E. A. From Rouse to Fully Established Entanglement Dynamics: A Study of Polyisoprene by Dielectric Spectroscopy. *Macromolecules* **2010**, *43*, 3340–3351.
- (48) Heck, M.; Schneider, L.; Müller, M.; Wilhelm, M. Diblock Copolymers with Similar Glass Transition Temperatures in Both Blocks for Comparing Shear Orientation Processes with DPD Computer Simulations. *Macromol. Chem. Phys.* **2018**, *219*, 1700559.
- (49) Fox, T. G.; Flory, P. J. Second-Order Transition Temperatures and Related Properties of Polystyrene. I. Influence of Molecular Weight. *J. Appl. Phys.* **1950**, *21*, 581–591.
- (50) Kipnusu, W. K.; Kossack, W.; Iacob, C.; Jasiurkowska, M.; Rume Sangoro, J.; Kremer, F. Molecular Order and Dynamics of Tris(2-ethylhexyl)phosphate Confined in Uni-Directional Nanopores. *Zeitschrift für Physikalische Chemie* **2012**, *226*, 797–805.
- (51) Imanishi, Y.; Adachi, K.; Kotaka, T. Further investigation of the dielectric normal mode process in undiluted cis -polyisoprene with narrow distribution of molecular weight. *J. Chem. Phys.* **1988**, *89*, 7585–7592.
- (52) Matsumiya, Y.; Watanabe, H.; Osaki, K. Comparison of Dielectric and Viscoelastic Relaxation Functions of cis -Polyisoprenes: Test of Tube Dilation Molecular Picture. *Macromolecules* **2000**, *33*, 499–506.
- (53) Sato, T.; Watanabe, H.; Osaki, K.; Yao, M.-L. Relaxation of Spherical Micellar Systems of Styrene-Isoprene Diblock Copolymers. I. Linear Viscoelastic and Dielectric Behavior. *Macromolecules* **1996**, *29*, 3881–3889.
- (54) Cziep, M. A.; Abbasi, M.; Heck, M.; Arens, L.; Wilhelm, M. Effect of Molecular Weight, Polydispersity, and Monomer of Linear Homopolymer Melts on the Intrinsic Mechanical Nonlinearity $^3Q_0(\omega)$ in MAOS. *Macromolecules* **2016**, *49*, 3566–3579.
- (55) Watanabe, H. Viscoelasticity and dynamics of entangled polymers. *Prog. Polym. Sci.* **1999**, *24*, 1253–1403.
- (56) Watanabe, H. Dielectric Relaxation of Type-A Polymers in Melts and Solutions. *Macromol. Rapid Commun.* **2001**, *22*, 127–175.
- (57) Vega, J. F.; Rastogi, S.; Peters, G. W. M.; Meijer, H. E. H. Rheology and reptation of linear polymers. Ultrahigh molecular weight chain dynamics in the melt. *J. Rheol.* **2004**, *48*, 663–678.
- (58) Colby, R. H.; Fetters, L. J.; Graessley, W. W. The melt viscosity-molecular weight relationship for linear polymers. *Macromolecules* **1987**, *20*, 2226–2237.
- (59) Fetters, L. J.; Lohse, D. J.; Milner, S. T.; Graessley, W. W. Packing Length Influence in Linear Polymer Melts on the Entanglement, Critical, and Reptation Molecular Weights. *Macromolecules* **1999**, *32*, 6847–6851.
- (60) Montfort, J. P.; Marin, G.; Monge, P. Effects of constraint release on the dynamics of entangled linear polymer melts. *Macromolecules* **1984**, *17*, 1551–1560.
- (61) Dalsin, S. J.; Hillmyer, M. A.; Bates, F. S. Molecular Weight Dependence of Zero-Shear Viscosity in Atactic Polypropylene Bottlebrush Polymers. *ACS Macro Lett.* **2014**, *3*, 423–427.
- (62) Dalsin, S. J.; Hillmyer, M. A.; Bates, F. S. Linear Rheology of Polyolefin-Based Bottlebrush Polymers. *Macromolecules* **2015**, *48*, 4680–4691.

Recommended by ACS

Vitrification of the Entire Amorphous Phase during Crystallization of Poly(butylene terephthalate) near the Glass-Transition Temperature

Akihiko Toda, Christoph Schick, *et al.*

APRIL 14, 2023

MACROMOLECULES

READ 

Associating Polymers in the Strong Interaction Regime: Validation of the Bond Lifetime Renormalization Model

Sirui Ge, Alexei P. Sokolov, *et al.*

MARCH 10, 2023

MACROMOLECULES

READ 

Combined Mixing and Dynamical Origins of T_g Alterations Near Polymer–Polymer Interfaces

Asieh Ghanekarade and David S. Simmons

DECEMBER 30, 2022

MACROMOLECULES

READ 

Microscopic versus Macroscopic Glass Transitions and Relevant Length Scales in Mixtures of Industrial Interest

Numera Shafqat, Juan Colmenero, *et al.*

FEBRUARY 28, 2023

MACROMOLECULES

READ 

Get More Suggestions >